
The timing and evolution of the post-glacial transgression across the Sea of Marmara shelf south of Istanbul

K. Eris^{a,*}, W.B.F Ryan^b, M.N. Çağatay^a, U. Sancar^a, G. Lericolais^c, G. Ménot^d, E. Bard^d

^aIstanbul Technical University Faculty Of Mines, Emcol, Geology Department Ayazağa, İstanbul Turkey

^bLamont-Doherty Earth Observatory of Columbia University, Palisades, NY, USA

^cLaboratoire de Environnements Sedimentaires, IFREMER, France

^dCollège de France, CEREGE, UMR-6635, France

*: Corresponding author : Eris K. email address : keris@itu.edu.tr

Abstract:

High-resolution reflection seismic profiles with core analyses of sedimentary sequence near the Sea of Marmara (SoM) entrance to the Strait of İstanbul (Sol, Bosphorus) provide detailed record of sealevel changes since the Late Glacial Maximum (LGM). The sequence is deposited over the LGM erosional surface at a maximum depth of -105 m. It includes seven seismic units that can be confidently correlated with 14C-dated sedimentary units in the cores. Unit 6 represents levee deposits of the paleo-Sol channel that was deposited by a Black Sea outflow during 11.2-10.6 kyr BP. The reflection surfaces at base of Unit 5 and 4 correspond to wave-cut terraces at -71 and -63 m, respectively, and are estimated to be 10.6 and 9.8 kyr BP. The seismic Unit 2, overlaying a mud drape (Unit 3), comprises deltaic sediments that was deposited during 6.400-3200 yr 14C BP. Isopach map and forset directions of the deltaic unit indicates that the delta was sourced from Kurbağalidere River. Depositional period of the delta is subdivided into two stages in response to changes in the 49 balance between sealevel change and sediment supply rates: a progradational and an aggradational stages. The progradational stage prevailed during 6.4-4.7 kyr BP when the sealevel rise decelerated and there was a high sediment input from the drainage area of the Kurbağalidere River. An aggradational stage developed during 4.7-3.2 kyr BP and indicates that the delta grew during faster sealevel rise when the rate of sediment input was relatively decreased. The onset of delta deposition at 6.4 kyr BP is marked in the SoM by termination of the early Holocene Sapropel deposition and the aggradational stage overlaps with the late Holocene Sapropelic unit deposited on the shelf areas. Our finding contradicts the hypothesis of Hiscott et al. (2002) and Aksu et al. (2002) that this delta was sourced from the Black Sea and that it indicates a persistent Black Sea outflow since 10 kyr BP.

Keywords: seismic stratigraphy; sealevel; Holocene; Marmara Sea; delta; sapropel

64 **1. INTRODUCTION**

65 The Sea of Marmara (SoM) is a 210 km long and 75 km wide intracontinental sea on
66 the gateway between the Mediterranean Sea and the Black Sea (Fig. 1). It is connected to the
67 low salinity ($S=18\%$) Black Sea via the Strait of Istanbul (SoI, Bosphorus) and to the marine
68 ($S=38\%$) Aegean Sea via the Çanakkale Strait (Dardanelles), having sill depths of -35 and -
69 75 m, respectively. The shelf break in the SoM occurs at ~90 m water depth. The SoI's
70 channel connects with a prominent submarine canyon dissecting the SoM shelf (Fig. 2).

71

72 During the late glacial sealevel lowstand, the SoM was isolated from the
73 Mediterranean Sea and it was a fresh to brackish water lake, as indicated by the presence of

74 the Neoeuxinian fauna in the SoM (Çağatay et al., 2000). With the rise of the sealevel as a
75 result of deglaciation, Mediterranean marine waters flooded the SoM at ca. 12 kyr BP
76 (Çağatay et al., 2000). Following this marine connection, the sealevel continued to increase in
77 the SoM, in tandem with the global sealevel. During the Younger Dryas (YD) there was a
78 sealevel still stand at -65 m in the SoM, as evidenced by a prominent palaeoshoreline and
79 erosional terrace over the Marmara shelves (Çağatay et al., 2003). Global ocean level
80 increased further during the Climatic Optimum starting at 10.5 cal. kyr BP (Derijk et al.,
81 1999). The Mediterranean waters from the SoM eventually flooded the Black Sea through the
82 SoI after breaching of the strait's sill at 8.4 kyr BP (Ryan et al., 2003; Major et al., 2002,
83 2004).

84 Two Holocene deltas are present on the both sides of the SoI on northern shelf of the
85 SoM (Fig.1). The one west of the SoI, is clearly sourced from the Ayamama River (Kurt,
86 1994) (Fig.1c); whereas the sediment source and timing of deposition for the other delta near
87 the SoM entrance of the SoI (Fig. 1d), close to the mouth of Kurbagalidere River, is
88 controversial. The latter delta has been studied by different workers to test the “catastrophic
89 Black Sea flooding at 7.2 kyr BP” hypothesis of Ryan et al. (1997). Hiscott et al. (2002) and
90 Aksu et al. (2002) proposed that the delta was constructed during 10-9 kyr BP by a Black Sea
91 outflow that persisted to the present. However, Major et al. (2002) and Ryan et al. (2003)
92 using isotope, seismic and bathymetric data concluded that the Black Sea outflow through SoI
93 occurred during the Younger Dryas (YD), which was followed by a drop in the level of the
94 Black Sea from -35 m to -95 m. The same delta was also studied by Oktay et al. (2002) and
95 Göktaşan et al. (2005) who concluded that it was sourced from the Kurbagalidere River, rather
96 than by the SoI and deposited during 11-10 kyr BP.

97

98 In this study, we present detailed seismic stratigraphic analysis of high resolution
99 shallow seismic lines crossing an area near the southern entrance of SoI, together with the
100 core stratigraphy. Our objectives are to discuss the chronostratigraphic evolution of the
101 Holocene sediments including delta formation in the paleo-SoI channel, and shed light on the
102 water exchange problem between the Marmara and the Black Seas during the Holocene.

103

104 **2. METHODS OF SEISMIC DATA ACQUISITION AND ANALYSIS**

105 The high-resolution profiles were obtained during two cruises of the Department of
106 Navigation, Hydrography and Oceanography (SHOD) R/V Çubuklu in 1993 and 1997 (Fig.
107 2). The sparker data were recorded directly on paper and covered approximately the top 100
108 m of the subsurface. Positioning was provided by Trisponder (using three shore-based radio
109 beacons) with an accuracy of about 10 m. Depths of reflectors were estimated using average
110 water and sediment velocities of 1500 and 1700 m.s⁻¹, respectively. The present day
111 bathymetric map of the southern entrance was created by using seismic profiles and
112 additional SHOD data (Fig. 2). Two gravity cores were recovered onboard R/V MTA Sismik-
113 1 in 2003 and R/V Marion Dufresne in 2004. Core TSU03-13 (40° 57' 20/ 29° 00' 09) is
114 located on the top of the delta at 37 m water depth on the eastern part of seismic profile K3
115 (Fig. 2). Core MD-2750 (40° 56' 70/ 28° 56' 15) is located in the submarine channel of the SoI
116 at 68 m water depth on the seismic profile K4 (Figs. 2 and 3).

117

118 The ages of reflectors A and B marking the termination and onset of the delta were
119 obtained by ¹⁴C dating of bivalve shells in gravity cores (Fig. 3; Table 1). The shells were
120 carefully cleaned to remove any coatings, and then studied under microscope to ensure that
121 they were diagenetically unaltered. The radiocarbon analysis was carried out at the University
122 of Arizona (Lab. Number A-13668) and Woodshole NOSAMS facility (Lab. Number OS-

123 50130, OS-50131 and OS-53538). The ages were calculated as yr BP, corrected for ^{13}C , and
124 errors are expressed as $\pm 1\sigma$. The ^{14}C ages are not corrected for the reservoir age and not
125 calibrated. Organic carbon (Corg) was analysed by the Walkey-Balke method (Gaudette et al.,
126 1974). The percentage of sand + silt fraction was determined by wet sifting of the samples
127 through 63 μm sieve. Physical property measurements were made on whole, unsplit sections
128 of Core MD-2750 using a Geotek Multi-Sensor Core Logger equipped with gamma density,
129 P-wave velocity and magnetic susceptibility sensors (Boyce, 1976; Gerland and Villinger,
130 1995; Breitzke, 2000).

131

132 **3. RESULT AND DISCUSSION**

133 *3.1. Seismic and core stratigraphy*

134 We identified eight reflector surfaces including the seafloor and seven seismic units
135 deposited during the late glacial maximum (LGM) to present (Fig. 4). Late glacial lowstand
136 unconformity surface is represented in the seismic profiles by reflection surface K (Figs. 4, 5
137 and 6), which extends into the shelf break at about -100 m. Lowermost seismic unit (Unit 7)
138 was therefore deposited over the truncation surface K during the deglaciation period (Fig. 4).
139 Lowermost part of the Unit 7 correlates with shoreface deposits formed during formation of a
140 wave-cut terrace at ca. -81 m on the eastern shelf of the paleo-strait's channel (Fig. 5). This
141 can be correlated with the 12 kyr BP old -85 m shoreline observed in different parts of the
142 SoM (Çağatay et al., 2003; Polonia et al., 2004). Reflection surface G truncates Unit 7 (Fig.
143 4), onto which Unit 6 was deposited. While the minimum depth of the reflector G is around -
144 80 m, the sealevel must be above during truncation of the Unit 7, therefore, approximate age
145 of this reflector can be estimated as 11.2 kyr BP according to global sealevel curves of
146 Fairbanks, (1989) and Sidall et al (2003).

147 Unit 6 consists of conformable beds constituting a ridge-like feature in the middle of
148 the main channel and dipping in opposite directions (Figs. 5 and 6). We interpret this unit as
149 a levee deposited in the main paleo-strait's channel. The lowermost 175 cm part of Core MD-
150 2750 represents the upper part of the levee deposit (Unit 6), which comprises silty and sandy
151 beds with marine molluscan shells (Figs. 3b and 7). This unit is differentiated from the
152 overlying other units by its relatively coarse-grained nature. Its sand + silt fraction in the
153 core amounts to 10-47% of the total sediment (Fig 8). The coarse-grained nature of the levee
154 sediments is also shown in the Gamma-density and P-wave velocity profiles, which show
155 normal grading in upper part of the unit (Fig. 9). Magnetic susceptibility values increase
156 towards to the top of the unit (and lower part of Unit 5) because of high clay input, probably
157 enhanced with a ferromagnetic component of diagenetic origin.

158

159 The levee unit is overlaid by Unit 5 over truncation surface E (Figs.4, 5 and 6), which
160 corresponds to the onset of the early Holocene Sapropel (Çağatay et al., 2000; Tolun et al.,
161 2002) as indicated by high Corg values (>1.5 wt%) and its stratigraphic position in Core MD-
162 2750 (Figs. 3b and 3c). This sapropelic layer was previously dated 10.6-6.4 kyr BP by
163 Çağatay et al. (2000). Its onset age is consistent with the ^{14}C ages of 10.95 kyr BP and 10.45
164 kyr BP obtained below and above truncation surface E, therefore, age of the reflector E can be
165 estimated as 10.6 kyr BP (Fig. 3b). Eastern part of the study area, reflector E is associated by
166 a formation of wave-cut terrace at -71 m (Fig. 6). Timing of this wave-cut terrace can be
167 estimated as 10.6 kyr BP, when the Early Holocene sapropel deposition began in the SoM. On
168 the basis of these chronostratigraphic data, we can tentatively estimate the age of Unit 6
169 between 11.2 and 10.6 kyr BP.

170

171 Unit 5 is characterized by moderately continuous, subparallel internal reflections
172 forming a mud drape accumulated over the levee deposits in the main paleo-strait's channel
173 (Fig. 4). In Core MD-2750, Unit 5 comprises marine shelly homogeneous clay in the lower
174 part and grades into finely parallel and cross laminated silt (Figs. 3b and 7). Transition from
175 Unit 6 to 5 is represented by a decreasing grain size that is shown in the Gamma density
176 measurement (Fig. 9). Despite the decreased grain size in the lower part of Unit 5 the P-wave
177 velocity is high probably due to a low porosity caused by core compaction. The upper parallel
178 and cross laminated part of Unit 5 is represented by a relatively low Gamma density, but high
179 P-wave velocity values because of the increased silt content (Fig. 9). Unit 5 is followed
180 upward by Unit 4 over unconformable reflection surface D (Fig. 4). Timing of this reflector
181 surface can be assigned to -63 m paleo-shoreline, while formation of a wave-cut terrace
182 truncated the sediment below reflector D on the eastern part of the main paleo-strait's channel
183 (Fig. 5). The erosion above Unit 5 is shown by a truncation of the laminations in Core MD-
184 2750 (Fig. 7).

185

186 Age of the -63 m shoreline from the global sealevel curves (Fairbanks, 1989 and Sidall
187 et al., 2003) can be estimated as ca. 10-9.8 kyr BP. The same reflector (surface D) was dated
188 by Aksu et al. (2002) as 9.8 kyr BP in the southern shelf of SoM, which is supported by the
189 global sealevel curves (Fairbanks, 1989 and Sidall et al., 2003) for this period. According to
190 chronostratigraphic relation of the underlying and overlying reflector surfaces of Unit 5, this
191 unit was deposited between 10.6-9.8 kyr BP. Unit 4 is characterized by mud drape in the main
192 paleo-strait's channel showing moderately continuous parallel internal reflectors (between
193 reflectors D and C in Figs. 5 and 6). It is associated by the formation of -63 m paleo-shoreface
194 deposits between reflectors D and C on the eastern part of the main paleo-strait's channel
195 (Fig. 6). The shoreface deposits indicate progradational clinoforms characterized by

196 acoustically strong internal reflectors. In Core MD-2750, Unit 4 comprises finely parallel and
197 cross laminated clayey silt with marine shell (Figs. 3b and 7). Seismic Unit 4 together with
198 Unit 3 correspond to the upper part of the early Holocene Sapropel layer as indicated by high
199 organic carbon value ($> 1.5\%$) (Fig. 3c).

200

201 Unit 3 overlies the progradational Unit 4 over reflection surface C (Fig. 4). It
202 represents laterally continuous, regularly reflective package of weak internal reflectors (Figs.
203 5 and 6). In Core MD-2750, Unit 3 consists of homogenous silty clay with marine molluscs
204 (Fig. 7). It is bounded at the top by reflection surface B, which corresponds to termination of
205 the early Holocene Sapropel (6.4 kyr BP, Çağatay et al., 2000; Figs. 3b and 3c). This is in
206 agreement with a ^{14}C age of 6460 yr BP obtained from the upper part of the Unit 3 (Figs. 3b
207 and 3c). We can bracket the age of the package including Units 4 and 3 between 9.8 and 6.4
208 kyr BP.

209

210 Unit 2 conformably overlay Unit 3 (Fig. 4), and consists of oblique clinofolds with
211 acoustically strong reflectors (Figs. 6 and 10) that represent the presence of delta foresets
212 composed probably of relatively coarse sediments. According to architectural features of the
213 foresets, the delta comprises lower progradational and upper aggradational parts (subunits 2a
214 and 2b) (Fig. 6). Offshore equivalent of Unit 2 is represented in Core MD-2750 by shelly
215 clayey silt in the lower part (subunit 2a) and silty clay with marine mollusc shells in the upper
216 part (subunit 2b; Figs. 3b and 9). Considering the Corg profile, the upper subunit (Unit 2a)
217 correlates with the late Holocene Sapropelic layer between 215-295 cm in the core (Fig. 3b
218 and 3c), having a depositional age of 4750-3200 yr BP (Çağatay et al., 1999). This shows that
219 the onset of the late Holocene Sapropelic layer corresponds to initiation of the aggradational
220 deltaic deposition ca. 4.7 kyr BP, and its termination can be correlated with the end of the

221 deltaic deposition ca. 3.2 kyr BP (Figs. 3b and 3c). Delta topset beds are represented in Core
222 TSU03-13 by pebbly sands with marine mollusc shells (Fig. 3a). An ^{14}C age of 4.4 kyr BP
223 was obtained in Core TSU03-13 near the upper part of the topset beds (Fig. 3a) that are
224 truncated by an overlying reflection surface A at -35 m (Figs. 6 and 10). The truncation
225 implies subaqueous erosion of the delta platform after termination of the delta deposition.
226 Considering the 4.4 kyr BP age from the delta topset and correlation with its upper part with
227 the late Holocene Sapropelic layer, the age of the deltaic unit (Unit 2) can be delimited
228 between 6.4 and 3.2 kyr BP. The delta deposits of Unit 2 is overlain by Unit 1 above
229 truncation surface A (Figs. 4 and 5).

230

231 The boundary between Units 2 and 1 is bioturbated in Core MD-2750, a typical
232 feature of sapropelic sediments (Figs. 7 and 10). Transition from Unit 2 to Unit 1 is indicated
233 by an abrupt increase in the magnetic susceptibility (Fig. 9). It seems that the Unit 2/Unit 1
234 boundary represents a redox front at the top of the sapropelic Unit 2, below which the
235 ferromagnetic component of the sediments is reduced and sulfidized.

236

237 Unit 1 consists of a package of moderately continuous and regular reflectors,
238 representing onlapping sediments over truncation surface A. In Core TSU03-13, Unit 1
239 consists of shelly and sandy silt intercalated with silty sand containing marine mollusc shells,
240 grades into clayey silt in the upper part (Fig. 3a). In the paleo-strait's channel, it is represented
241 by clay with marine shells infilling the topographic irregularities (Figs. 3b, 5 and 6).

242

243 *3.2. Kurbağalıdere River: its drainage area and water and sediment discharges*

244 Present day Kurbağalıdere River has several small tributaries, draining a total area of
245 46 km² with a steep topography (Fig. 11). The drainage area consists mainly of schist,

246 greywacke, limestone and quartzite of Palaeozoic age and Neogene sand and gravel. The
247 highest elevation of the catchment area is around 180 m. Present day mean discharge rate is
248 about 80 m³/yr (DSİ İstanbul, unpublished data). Suspended sediment load of Kurbağalıdere
249 River has not been measured. We estimated this load to be around 60, 000 ton/yr based on the
250 data of other rivers in the southern Marmara region (Table 2; EİE, 1993). We accept this
251 value to be also representative of the pre-anthropocene period. In the Marmara region, it is
252 estimated that total sediment flux of rivers to be 35% more than the measured suspension
253 sediment flux because of retention behind reservoirs and additional bedload (EİE, 2000;
254 Kazancı et al., 2004). The bedload constitutes about 10% of the total sediment influx
255 (Milliman and Mead, 1983). The total sediment retained behind dams and the bedload is
256 assumed to balance the opposite effects of deforestation and cultivation, based on the
257 conclusion of Svitski et al (2005) that the opposite effect of different human activities on the
258 sediment yield on a global scale is almost in balance.

259

260 *3.3. Evolution of the Delta*

261 Source and depositional period of the delta can be confidently deduced from the
262 correlation of the seismic stratigraphic units with the chronostratigraphic units in the cores.
263 The seismic units identified by us and Hiscott et al. (2002) can be correlated, while two sets
264 of profiles used by Hiscott et al (2002) and this study cross each other at the intersections
265 (Fig. 2). Seismic interpretations of both studies can be compared and correlated with high
266 confidence (Figs. 2 and 12). Seismic stratigraphic Units 2 and 3 of this study corresponds to
267 the deltaic unit (Unit 2 between $\beta 1$ and $\beta 2$ reflectors) of Hiscott et al. (2002). Unit 3 defined
268 by us is clearly not a part of the delta, because the delta foresets downlap onto reflector B
269 lying above Unit 3 (Figs. 6 and 10). This important disparity in the seismic interpretation,
270 produces significant differences in the delta isopach maps of the two studies (Fig. 13). Our

271 isopach map shows the presence of a delta lobe extending southwestwards, with the thickest
272 part of the delta (20 and 22 m thickness contours) located close to the mouth of the
273 Kurbağalıdere River (Fig. 13). The delta foresets dip at an average of 7° not only towards SW,
274 but also towards W and SE, radially diverging from the Kurbağalıdere River's mouth and
275 having true dips of up to 12° (Fig. 13). This delta geometry strongly suggests that the delta is
276 sourced from the Kubagalidere River. The delta also extends northwards towards the SoI.
277 This northward extension is because of the strong outflow of the Mediterranean water to the
278 Black Sea through the SoI, which started about 8.4 kyr BP (Major et al., 2002, Ryan et al.,
279 2003). Such an outflow could easily redistribute the deltaic sediments further north of the
280 Kurbağalıdere River mouth. There is no other river of reasonable size in the north of the
281 Kurbağalıdere River to cause a northward extension of the delta from the river's mouth (Fig.
282 8). A similar transport mechanism by the undercurrent has been suggested for the formation
283 of the -35 m southern sill of the Bosphorus by Algan et al. (2001). There, the sediment input
284 by the Alibeyköy and Kağıthane into the Golden Horn estuary was eventually transported
285 northwards into the strait's channel and piled up between Dolmabahçe and Üsküdar to form the
286 southern sill (see Fig. 1b).

287

288 In addition to the above facts, there are three other important lines of evidence against
289 the persistent Black Sea outflow origin of the delta as proposed by Hiscott et al. (2002) and
290 Aksu et al. (2002). First, the source of sediments of such an outflow delta is unexplained. The
291 sediment derived from land on either side of the SoI's channel would be trapped in the -80 m
292 deep, sediment-starved depressions along the SoI's channel, such as the Beykoz and Bebek
293 basins (Göktaşan et al., 1997; Algan et al., 2001). In contrast to Black Sea outflow hypothesis
294 of Hiscott et al (2002), formation of levee deposits in the paleo-SoI channel indicates that a
295 Black Sea outflow took place during 11.2-10.6 kyr BP according to our seismic and core data.

296

297 Second, according to the contour maps of both overlying and underlying reflectors (A
298 and B in Fig. 4) of the deltaic deposits, there was southwards flows of the paleo-strait's
299 channel before the onset and after termination of the delta (Figs. 14 and 15). Instead a delta
300 proposed to have been formed by a Black Sea outflow during 10-9 kyr BP would be expected
301 near the edge of the shelf at a water depth of 65 m. However, the contour map of the reflector
302 B (underlying delta deposits) shows that paleo-bathymetry before the onset of the delta was
303 considerably smooth (Fig. 14). This indicates that Kurbağalıdere River was in its backfilling
304 phase because high rate of sealevel rise that gave rise to further incursion of the sea into the
305 river valley untill sealevel rise slowed down at ca. 6.4 kyr BP. In contrast, the contour map of
306 the reflector A shows that there was still channellizing from the Kurbağalıdere River although
307 deltaic deposition was terminated (Fig. 15). After the delta deposition was ceased, the amount
308 of sealevel rise might have been relatively faster for delta deposition on the shelf area even
309 there was still sediment influx from the Kurbağalıdere River. After termination of the delta
310 deposition, the channel transect of the Kurbağalıdere River is well adjusted with the spreading
311 of the deltaic deposits, clearly showing source of the delta (Figs. 13 and 15). Third, the base
312 of the subaqueous delta is above -50 m which at a much higher elevation of the sealevel ca.
313 10 kyr BP, which was at ca. -65 m according to the global sea level curves (Fairbanks, 1989;
314 Siddal et al., 2003).

315

316 Based on the seismic stratigraphic and chronostratigraphic core analysis, the period of
317 the delta formation (6.4-3.2 kyr BP) determined by this study is in disagreement with 10-9 kyr
318 BP age given by Hiscott et al. (2002) and 11-10 kyr BP by Gökaşan et al. (2005). Hiscott et
319 al. (2002) determined the age of delta from a 1.25 m long core (MAR98-09 in Fig 13) that is
320 supposed to include the whole delta unit between reflectors β_1 and β_2 . The delta unit as

321 defined by Hiscott et al. (2002) includes older sediments (Unit 3 in this study) which is
322 clearly not a part of the delta. Moreover, Gökaşan et al. (2005) used shallow seismic lines on
323 the northern shelf and correlated the seismic units with a drill-hole section in the
324 Kurbağalidere River valley to discuss the source and age of the delta. They obtained an
325 electron spin resonance (ESR) age of $11,000 \pm 1100$ yr BP for an unconformity at -18 m, which
326 they consider to represent the onset of delta deposition during the Younger Dryas. This age
327 has a large error margin and is not compatible with the global sealevel of -75 to 65 m
328 (Fairbanks, 1989 and Sidall et al., 2003) for that time period.

329

330 We propose the following sequence of events leading to the delta formation.
331 According to global sealevel curves (e.g. Fairbanks, 1989 and Sidall et al. 2003), the rate of
332 sealevel rise decreased after ca. 6.5 kyr BP. This decrease combined with an increase in
333 sediment supply during mid-Holocene climatic optimum resulted in the deltaic progradational
334 sedimentation on the shelf of southern entrance of SoM to SoI. This conclusion is in
335 agreement with the fact that the mid-Holocene is a well known period for widespread delta
336 development (Stanley and Hait, 2000). The change from the progradational stage to the
337 aggradational stage of delta development at 4.7 kyr BP is marked by a relatively rapid rise of
338 sealevel as indicated by climbing delta foreset-topset transition (Fig. 6). The onset of
339 aggradational period also coincides with establishment of the present dual-flow regime
340 (Çağatay et al., 2000; Algan et al., 2001) with the Mediterranean under-current in the SoI,
341 forming a northward sediment drift. The delta deposition was terminated when increased base
342 level due to further global sealevel rise combined with a probable decrease in sediment input
343 by the Kurbağalidere River at ca 3.2 kyr BP. This date is supported by the correlation with the
344 age of the late Holocene Sapropel layer and by a ^{14}C age of 4.4 kyr BP in Core TSU03-13
345 below the eroded uppermost topset bed (Fig. 3a). The Kurbağalidere River, with a present

346 day annual water and sediment discharges of 80 m³ and 60.000 tons (EİE, 1993) draining a
347 180 m high ground southeast of the SoI, is large enough to form such a delta having about
348 290 x 10⁶ tons of sediment.

349

350

351 **4. CONCLUSIONS**

352 Seismic-stratigraphic and chronostratigraphic analyses near SoM entrance of the SoI
353 provide important information on sealevel changes since the LGM. The sedimentary sequence
354 in this area is deposited over the LGM a erosional surface and includes seven seismic units
355 that can be confidently correlated with ¹⁴C-dated chronostratigraphic units in the cores. In the
356 paleo-SoI channel, there is levee representing Unit 6 that implies a Black Sea outflow during
357 11.2-10.6 kyr BP. The reflection surfaces at base of Unit 5 and 4 are wave-cut platforms at -
358 71 and -61 m, corresponding to sealevel still stand periods around 10.6 and 9.8 kyr BP.

359

360 The seismic unit 2 is interpreted as a deltaic deposits. The isopach map of this delta
361 unit, together with the delta foreset dips, shows that the source of the deltaic sediments is
362 Kurbagalidere River draining a 46 km² topographically high area southeast of the SoI. The
363 progradational delta deposition started ca 6.4 kyr BP when rate of sealevel rise slowed down
364 and sediment input increased during the mid-Holocene climatic optimum until 4.7 kyr BP.
365 The progradational stage of delta deposition was followed by an aggradational stage during
366 4.7-3.2 kyr BP, which is characterized by a climbing topset-foreset transition. During this
367 second stage of delta development the rate of sealevel rise and sediment input were relatively
368 high. The onset of the aggradational delta stage corresponds in time to the establishment of
369 the present day dual-flow regime in the SoI and deposition of a sapropelic sediment layer on
370 the shelf areas of the SoM. Our findings contradict the Hiscott et al's (2002) hypothesis that

371 this delta was sourced from the Black Sea and that it indicates a persistent Black Sea outflow
372 since 10 kyr BP.

373

374

375

376 **References**

377 Aksu, A.E., Hiscott, R.N., Kaminski, M.A., Mudie, P.J., Gillespie, H., Abrojano, T., Yaşar,

378 D., 2002. Last glacial-Holocene paleoceanography of the Black Sea and Marmara Sea:

379 stable isotopic, foraminiferal and coccolith evidence. *Mar. Geol.* 190, 119-149.

380 Algan, O., Çağatay, M.N., Tchepalyga, A., Ongan, D., Eastoe, C., Göktaşan, E., 2001.

381 Stratigraphy of the sediment infill in Bosphorus Strait: water exchange between the Black

382 and Mediterranean Seas during the last glacial-Holocene. *Geo-Mar. Lett.* 20, 209-218.

383 Boyce, R.E., 1976. Definitions and laboratory techniques of compressional sound velocity

384 parameters and wet-water content, wet-bulk density, and porosity parameters by gravimetric

385 and gamma-ray attenuation techniques. In Schlanger, S.O., Jackson, E.D., et al., *Init.*

386 *Repts. DSDP, 33: Washington (U.S. Govt. Printing Office), 931-958.*

387 Breitzke, M., 2000. Physical properties of Marine Sediments. In Schulz, H.D. and Zabel, M.

388 (Eds.), *Marine Geochemistry*, Springer-Verlag Berlin Heidelberg New York, p 29-72.

389 Çağatay, M.N., Algan, O., Sakıncı, M., Eastoe, C., Egesel, L., Balkıs, N., Ongan, D., Caner,

390 H., 1999. A late Holocene sapropelic sediment unit from the southern Marmara shelf and its

391 palaeoceanographic significance. *Quater. Geol. Rev.* 18, 531-540.

392 Çağatay, M.N., Görür, N., Algan, A., Eastoe, C.J., Tchepalyga, A., Ongan, D., Kuhn, T.,

393 Kuşcu, İ., 2000. Late Glacial-Holocene palaeoceanography of the Sea of Marmara: timing

394 of connections with the Mediterranean and the Black Sea. *Mar. Geol.* 167, 191-206.

395 Çağatay, M.N., Görür, N., Polonia, A., Demirbağ, E., Sakınç, M., Cormier, M.-H., Capotondi,
396 L., McHugh, C., Emre, Ö., Eriş, K., 2003. Sealevel changes and depositional environments
397 in the İzmit Gulf, eastern Marmara Sea, during the late glacial-Holocene period. *Mar.*
398 *Geol.* 202, 159-173.

399 De Rijk, S., Rohling, E.J., Hayes, A., 1999. Onset of climatic deterioration in the eastern
400 Mediterranean around 7 ky BP; micropaleontological data from Mediterranean sapropel.

401 EİE., 1993. Sediment data and sediment transport amount for surface water in Turkey.
402 Türkiye Elektrik İşleri Etüd Dairesi Genel Müdürlüğü, Ankara, EIE Publ. No.68.

403 EİE., 2000. Türkiye akarsularında suspanse sediment gözlemleri ve sediment taşınım
404 miktarları (Suspended sediment data and sediment transport amount for surface waters in
405 Turkey). EİEİ Genel Müdür. Yayın., 17-20 (Ankara).

406 Gaudette, H., Flight, W., Tones, L., and Folger, D., 1974. An inexpensive titration method for
407 the determination of organic carbon in recent sediments. *J. Sediment. Petrol.* 44, 249-253.

408 Gerland, S., and Villinger, H., 1995. Nondestructive density determination on marine
409 sediment cores from gamma-ray attenuation measurements. *Geo-Mar. Lett.* 15: 111-118.

410 Gökaşan, E., Demirbağ, E., Oktay, F. Y., Ecevitoğlu, B., Şimşek, M., Yüce, H. 1997. On the
411 origin of the Bosphorus. *Mar. Geol.* 140, 183-199.

412 Gökaşan, E., Algan, O., Tur, H., Meriç, E., Türker, A., Şimşek, M., 2005. Delta formation at
413 the southern entrance of Istanbul Strait (Marmara sea, Turkey): a new interpretation based
414 on high-resolution seismic stratigraphy. *Geo-Mar. Lett.* 25, 370-377.

415 Fairbanks, R.G., 1989. A 17,000-year Glacio-Eustatic sea level record: influence of glacial
416 melting rates on the Younger Dryas event and deep-ocean circulation. *Nature* 342, 637-
417 642.

418 Hiscott, R. N., Aksu, A. E., Yasar, D., Kaminski, M. A., Mudie, P. J., Kostylev, V. E.,
419 MacDonald, J. C. Isler, F.I., Lord, A. R., 2002. Deltas south of the Bosphorus Strait record
420 persistent Black Sea outflow to the Marmara Sea since ~10 ka, *Mar. Geol.* 190, 95-118.

421 Kazancı, N., Leroy, S., Ileri, Ö., Emre, Ö., Kibar, M., Öncel, S., 2004. Late Holocene erosion
422 NW Anatolia from sediments of Lake Manyas, Lake Ulubat and the southern shelf of the
423 Marmara Sea, Turkey. *Catena* 57, 277-308.

424 Kurt, H., 1994. Interpretation of high resolution seismic data offshore Yedikule-
425 Büyükçekmece (İstanbul) (in Turkish). İTÜ MSc thesis, 80 p.

426 Major, C., Ryan, W. Lericolais, G., Hajdas, I., 2002. Constraints on Black Sea outflow to the
427 Sea of Marmara during the last glacial–interglacial transition, *Mar. Geol.* 190, 19-34.

428 Major, C.O., Vidal, L., Cagatay, N., Goldstein, S.L., Ryan, W.B.F., Ménot-Combes, G., Bard,
429 E., Labeyrie, L., 2004. Comparison of isotopic records from the Marmara and Black Seas:
430 Indications of marine connection, outflow and exchange. EGU 1st General Assembly, 25-
431 30 April 2004, Nice, France.

432 Milliman, J.D., and Meade, R.H., 1983. World-wide delivery of river sediment to the oceans,
433 *J. Geology* 91 (1), 1-21.

434 Oktay, F.Y., Gökaşan, E., Sakıncı, M., Yaltrak, C., İmren, C., Demirbağ, E., 2002. The effects
435 of the North Anatolian Fault Zone on the latest connection between Black Sea and Sea of
436 Marmara, *Mar. Geol.* 190, 367-382.

437 Polonia, A., Gasperini, L., Amorosi, A., Bonatti, E., Bortoluzzi, G., Çağatay, N., Capotondi,
438 L., Cormier, M.-H., Görür, N., McHugh, C., Seeber, L. 2004. Holocene slip rate of the
439 North Anatolian Fault beneath the Sea of Marmara. *Earth and Planet. Sci. Lett.* 227, 411-
440 426.

441 Ryan, W. B. F., Pitman III, W.C., Major, C.O., Shimkus, K., Moskalenko, V., Jones, J. A.,
442 Dimitrov, P., Görür, N., Sakıncı, M. and Yüce, H., 1997. An abrupt drowning of Black Sea
443 shelf. *Mar. Geol.* 138, 119-126.

444 Ryan, W.B.F., C. Major., Lericolais, G. and S.L., Goldstein., 2003. Catastrophic Flooding Of
445 the Black Sea. *Annu. Rev. Earth Planet. Sci.* 31, 525-554.

446 Siddall, M., Rohling, E.J., Almog-Labin, A., Hemleben, Ch., Melschner, D., Schmelzer, I.,
447 Smeed, D.A. 2003. Sea-level fluctuations during the last glacial cycle. *Nature* 243, 853-
448 858.

449 Stanley, D.J. and Hait, A.K., 2000. Deltas, radiocarbon dating, and measurements of sediment
450 storage and subsidence. *Geology* 24, 295-298.

451 Syvitski, J.P.M., Vörösmarty, C.J., Kettner, A.J., Green, P., 2005. Impact of human on the
452 flux of terrestrial sediment to the global coastal ocean. *Science* 308, 376-380.

453 Tolun, T., Çağatay, M.N., Carrigan, W.J., 2002. Organic geochemistry and origin of
454 Holocene sapropelic layer and associated sediments in Marmara Sea. *Mar. Geol.* 190, 47-
455 60.

456

457

458

459

460

461

462

463

464

465

466

467

468

469

470

471 **Figure Captions**

472 Fig. 1. Bathymetric map of the Sea of Marmara (SoM) (a). Inset maps: (b) southern entrance
473 of the Strait of Istanbul (SoI) and Golden Horn, (c) bathymetry of Bakırköy shelf, (d) SoI's
474 entrance to the SoM showing studied seismic profiles. Contours are in meters.

475

476 Fig. 2. Present bathymetric map of Sea of Marmara entrance of the İstanbul Strait created by
477 using seismic profiles and additional SHOD data. It shows seismic profiles and gravity cores
478 studied in this study. Broken lines are the seismic profiles were studied by Hiscott et al.
479 (2002).

480 Fig. 3. Lithological logs of the gravity cores TSU03-13 (a), MD-2750 (b), and organic carbon
481 (Corg) distribution in Core MD-2750 (c). Letters A to E denote the seismic reflectors
482 bounding seismic units 1-6, which are correlated with the lithological units.

483

484 Fig. 4. Generalized seismic stratigraphic units in the seismic profiles defined by this study and
485 their depositional facies observed in paleo-channel of SoI and on shelf.

486

487 Fig. 5. High-resolution seismic profile K4 showing wave-cut terraces at -81 m and -63 m and
488 a levee deposit between G and E reflectors. It also shows location of Core MD-2750
489 intersecting the uppermost part of the levee deposits. Prograded shoreface sediments are

490 delimited by reflectors K-G and D-C. Seismic reflectors of B, D, E, G and K are erosional
491 surfaces that truncate the underlying beds.

492

493 Fig. 6. High-resolution seismic profile K2 showing formation of wave-cut terrace at -71 m
494 and shoreface sediments of -63 m paleoshoreline. Deltaic deposit comprises lower
495 progradational and upper aggradational foreset beds between B and A reflector surfaces.

496 Seismic reflectors of B, D, E, G and K are erosional surfaces that truncate the underlying
497 beds.

498

499 Fig. 7. Photos of Core MD-2750 showing differentiated lithostratigraphic units and their
500 litologic and stratigraphic features. Letters A to E denote the seismic reflectors bounding
501 seismic units 1-6, which are correlated with the lithological units. S1-S9 are section numbers
502 of the splitted core and S1 is the uppermost section of the core.

503

504 Fig.8. The percentage of sand + silt fraction in Core MD-2750 determined by wet sifting of
505 the samples through 63 μm sieve.

506

507 Fig. 9. Lithologic log of Core MD-2750 (a) and physical property measurements made on
508 unsplit sections of the core using a Geotek Multi-Sensor Core Logger (b).

509

510 Fig. 10. High-resolution seismic profile K3 showing delta deposits bound by reflectors A and
511 B, and location of Core Tsu03-13 intersecting the delta topset. Notice the delta forsets dipping
512 in opposite directions and topsets truncated at -35 m.

513

514 Fig. 11. Topographic map of the catchment area of the Kurbağaldere River.

515

516 Fig. 12. Correlation of the chronostratigraphy of the seismic stratigraphic units defined by this
517 study and Hiscott et al. (2002). The delta unit corresponds to Unit 2 in this study and Units 2
518 and 3 in Hiscott et al.'s study.

519

520 Fig. 13. Comparison of isopach maps obtained by this study (continuous lines) and Hiscott et
521 al. (2002) (dashed lines). Circles in a different symbol show locations of the cores used by
522 this study (Tsu03-13 and MD2750) and by Hiscott et al. (2002) (MAR98-09). Note the arrows
523 indicating the true dip direction of the delta foresets. The isopach contours are in meters.

524

525 Fig. 14. Contour map of the reflector B showing paleo-bathymetry of the southern entrance
526 of the SoI prior to delta deposition. The contours are in meters.

527

528 Fig. 15. Contour map of the reflector A showing paleo-bathymetry of the southern entrance
529 of the SoI after delta deposition ceased. The contours are in meters.

530

Figure 1
[Click here to download high resolution image](#)

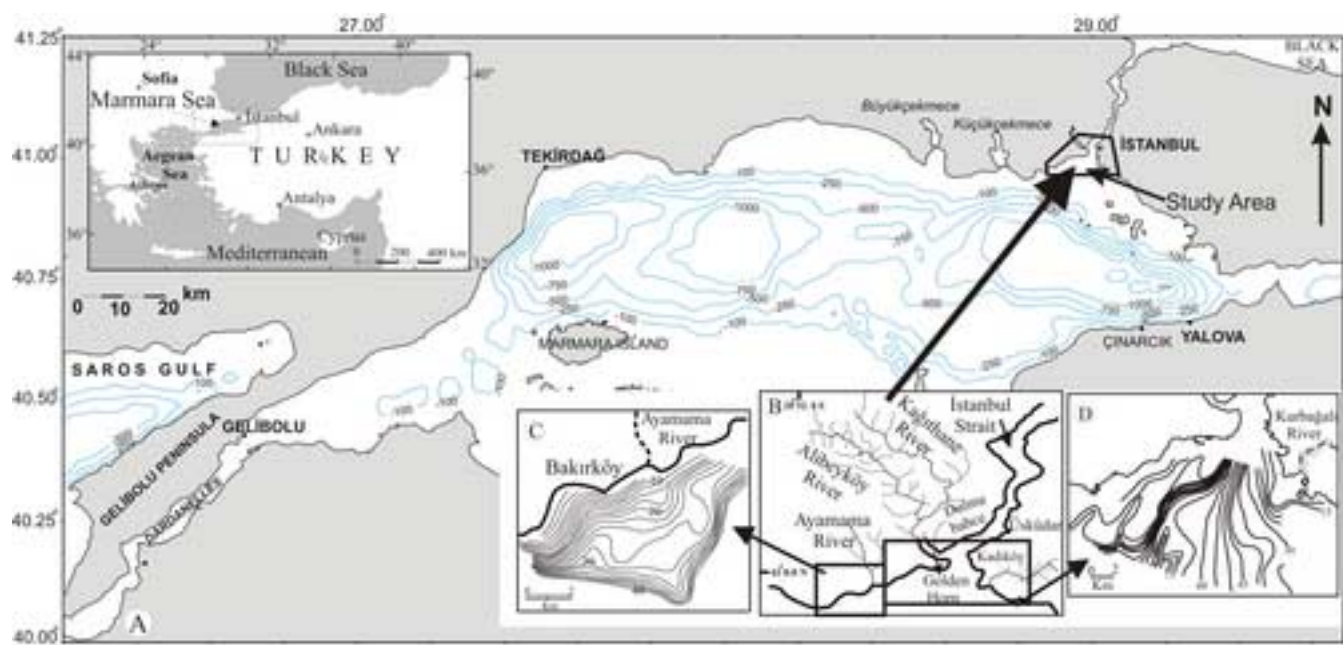


Figure 1

Figure 2
[Click here to download high resolution image](#)

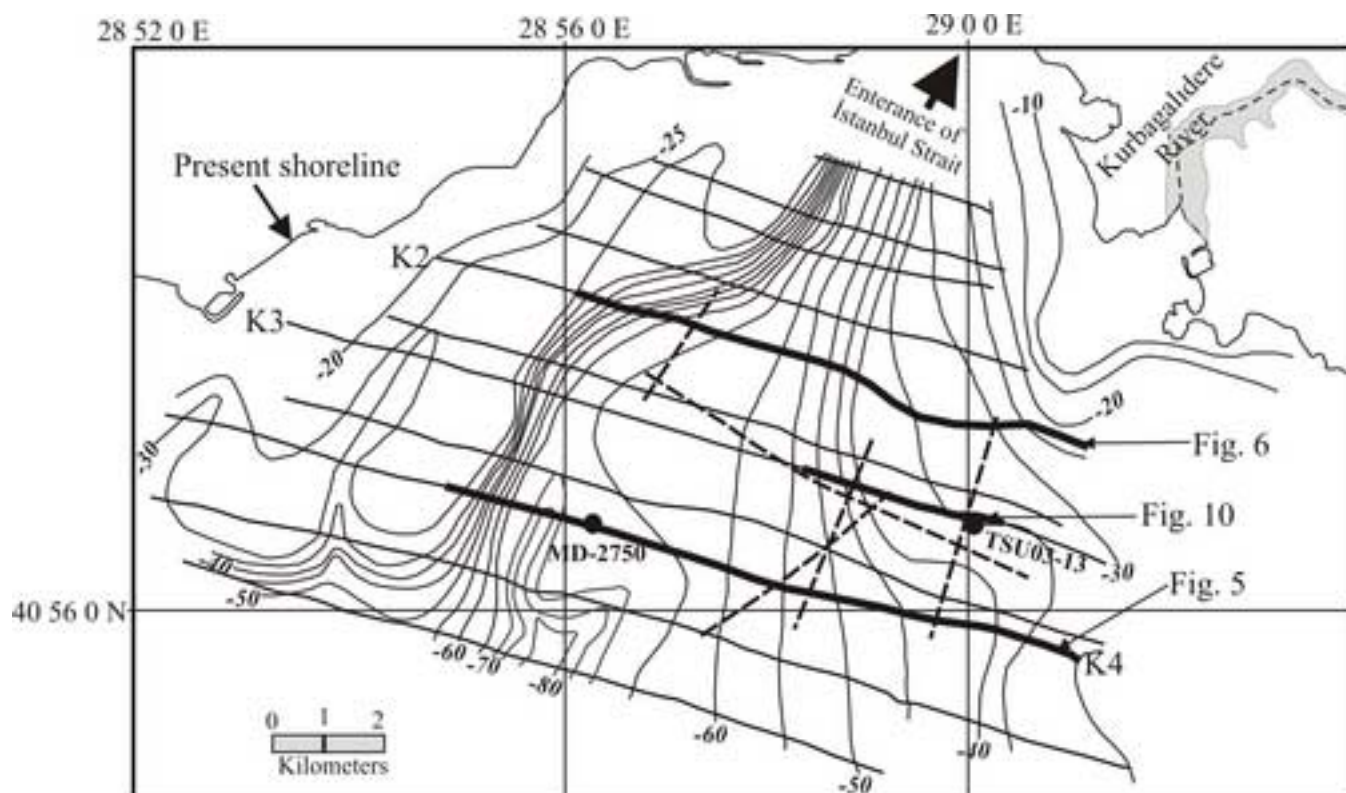


Figure 2

Figure 3
[Click here to download high resolution image](#)

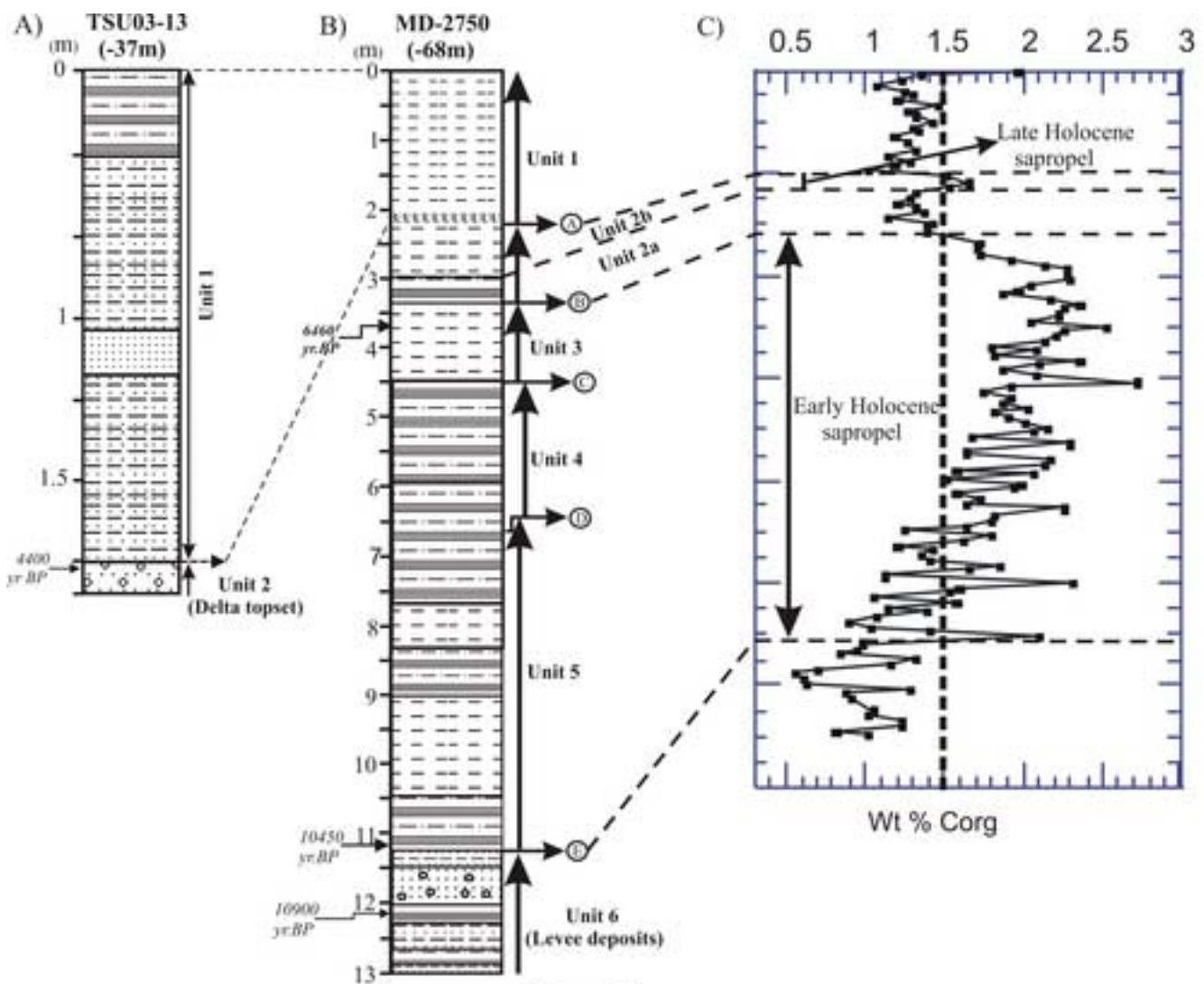


Figure 3

Figure 4
[Click here to download high resolution image](#)

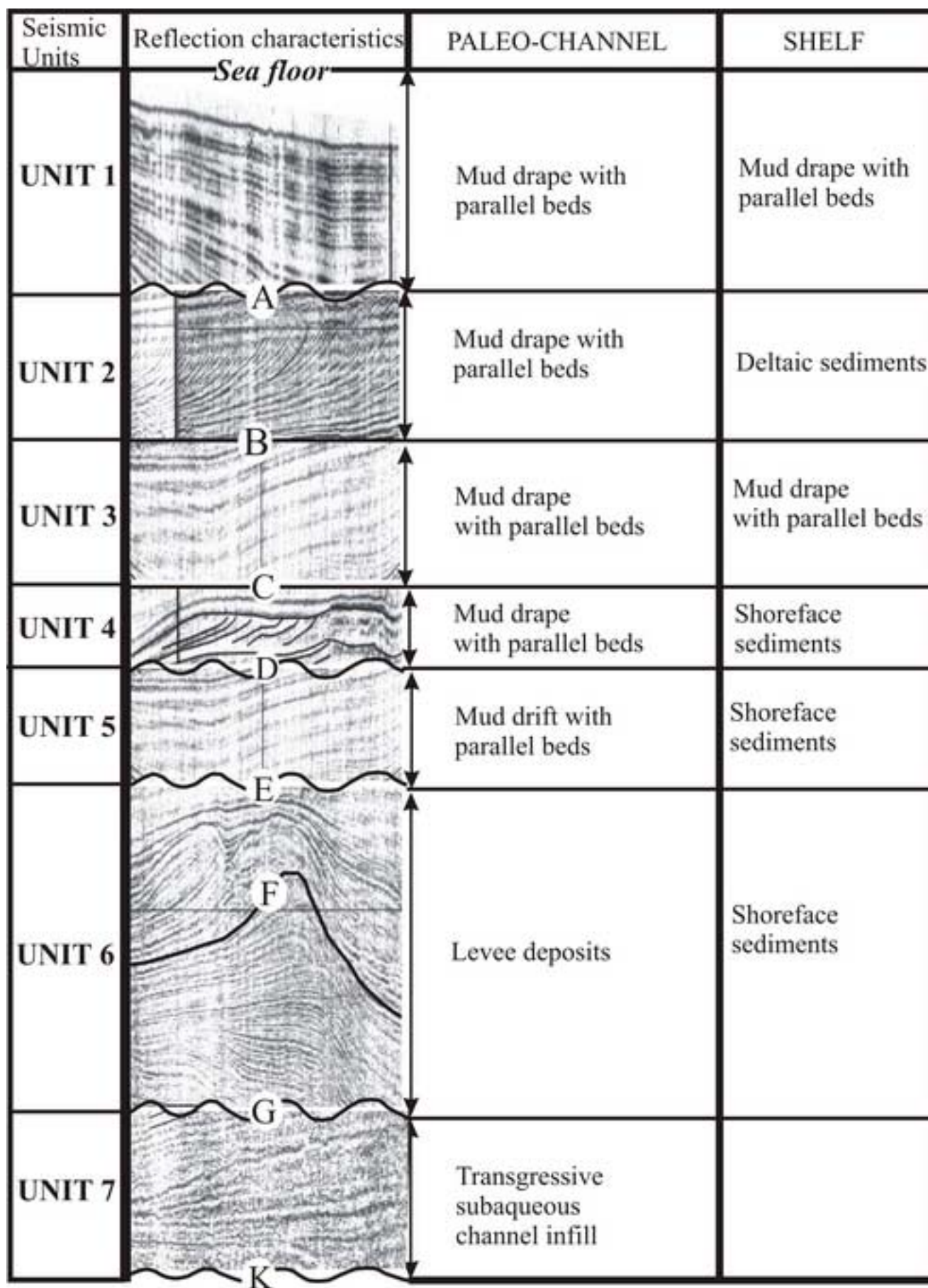


Figure 4

Figure 5
[Click here to download high resolution image](#)

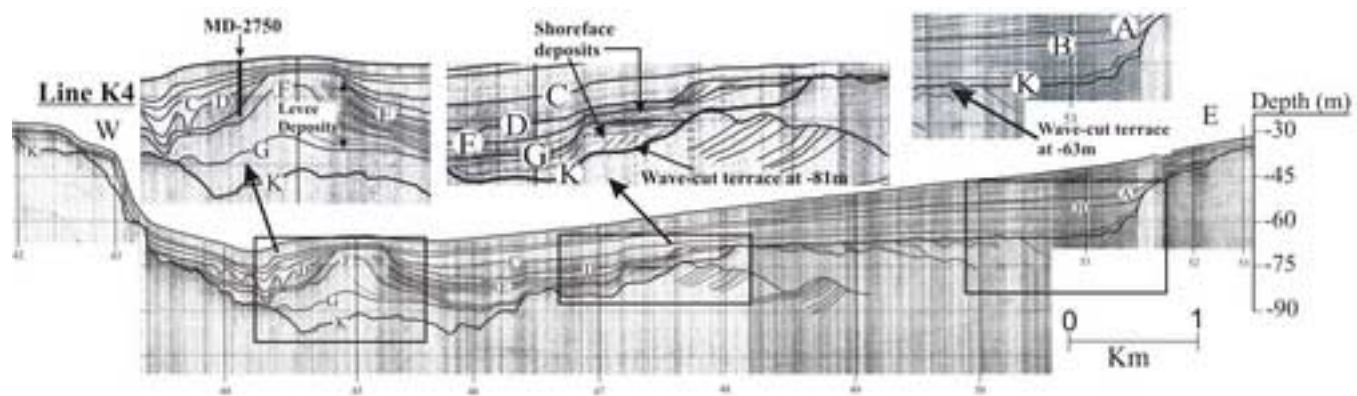


Figure 5

Figure 6
[Click here to download high resolution image](#)

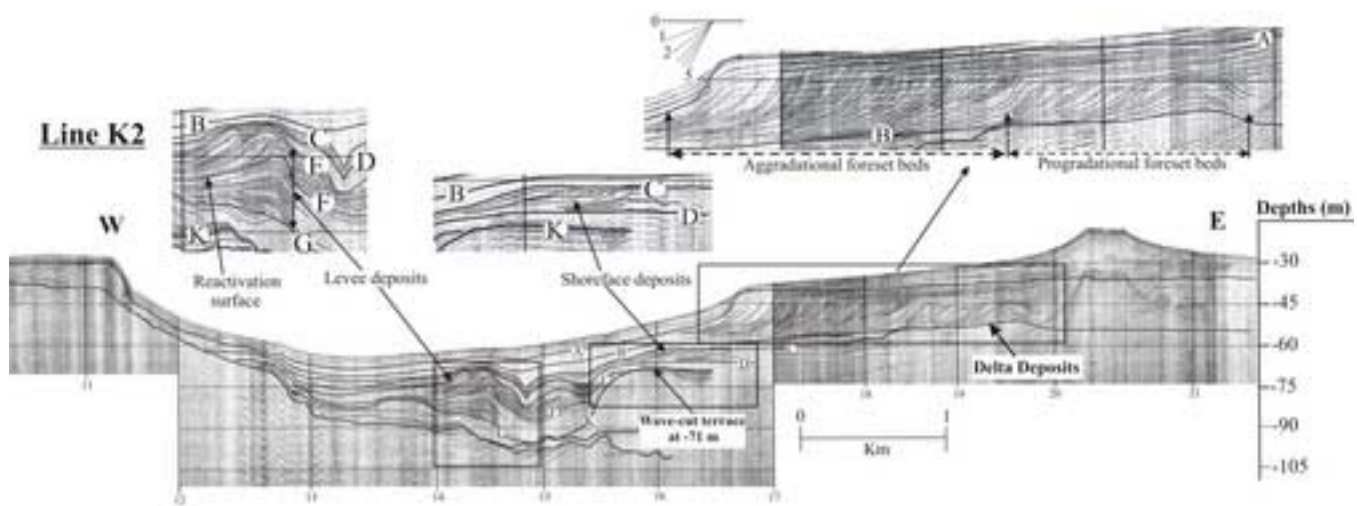


Figure 6

Figure 7
[Click here to download high resolution image](#)

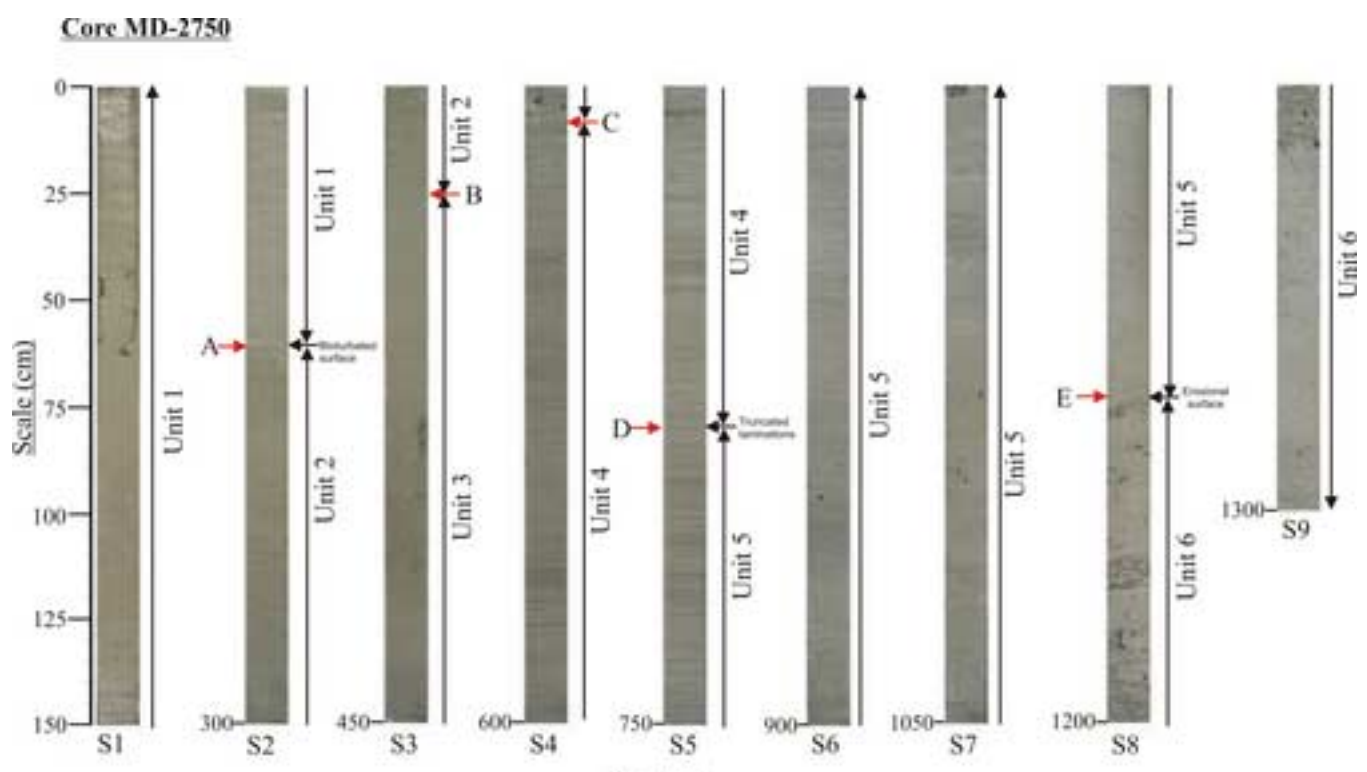


Figure 7

Figure 8
[Click here to download high resolution image](#)

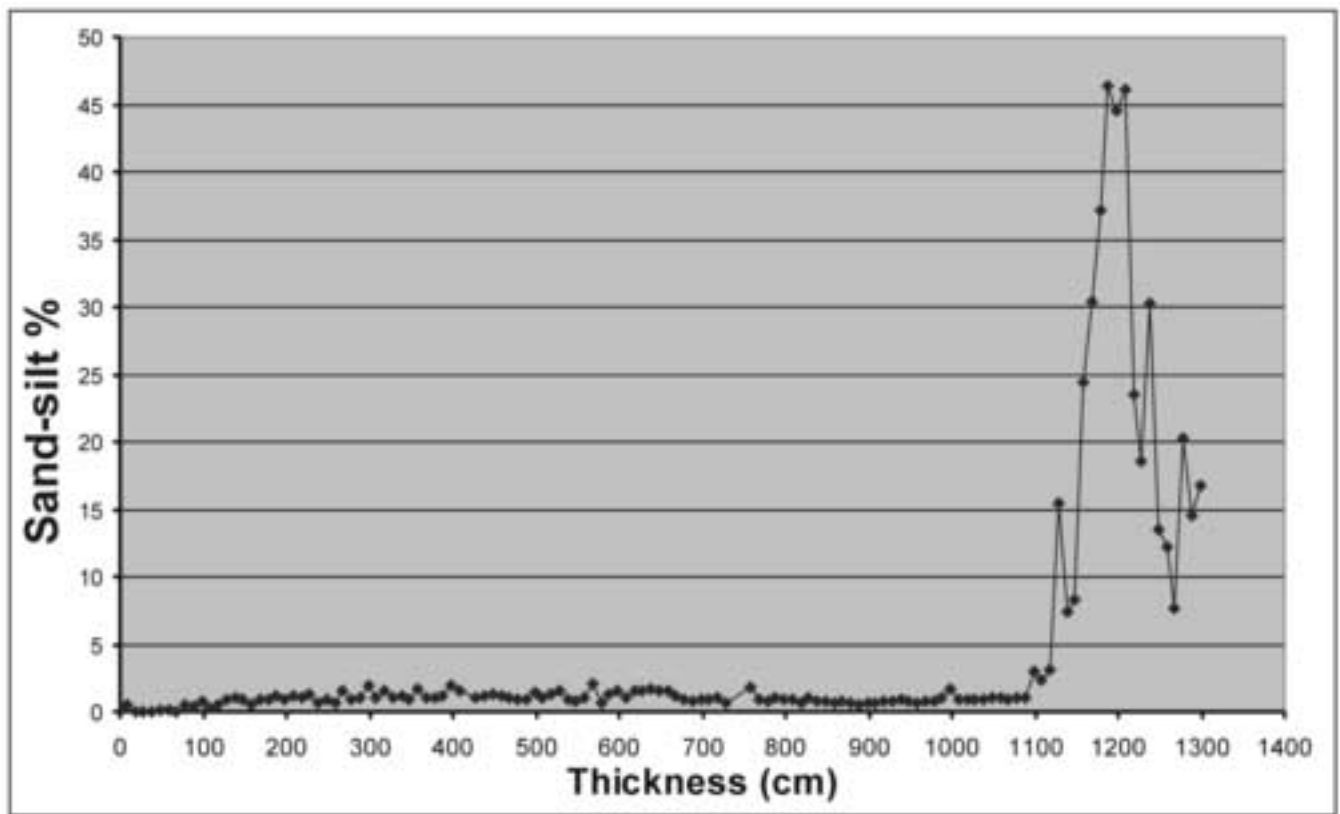


Figure 10
[Click here to download high resolution image](#)

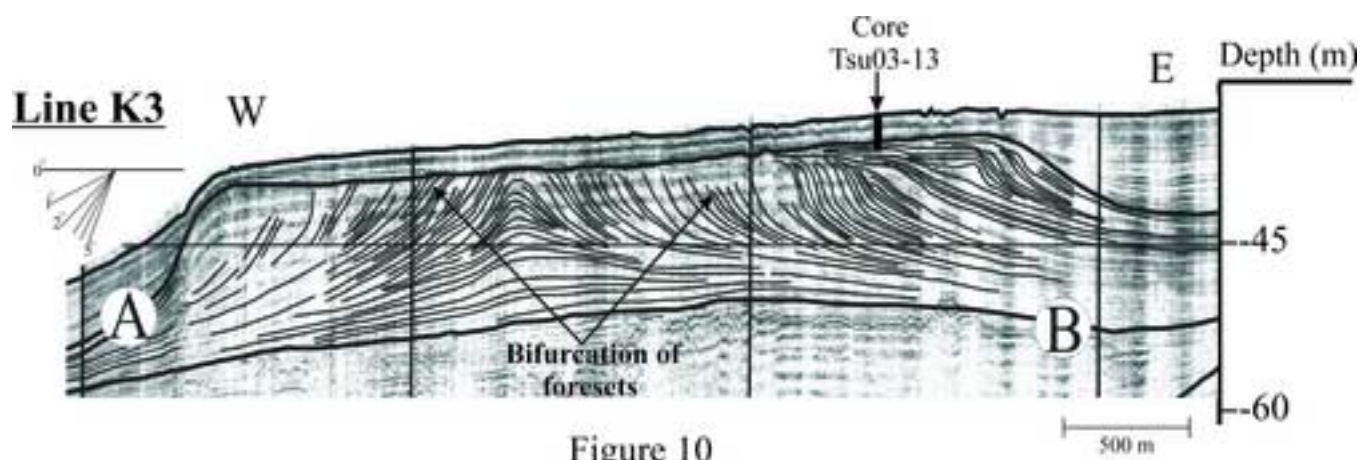


Figure 10

Figure 11
[Click here to download high resolution image](#)

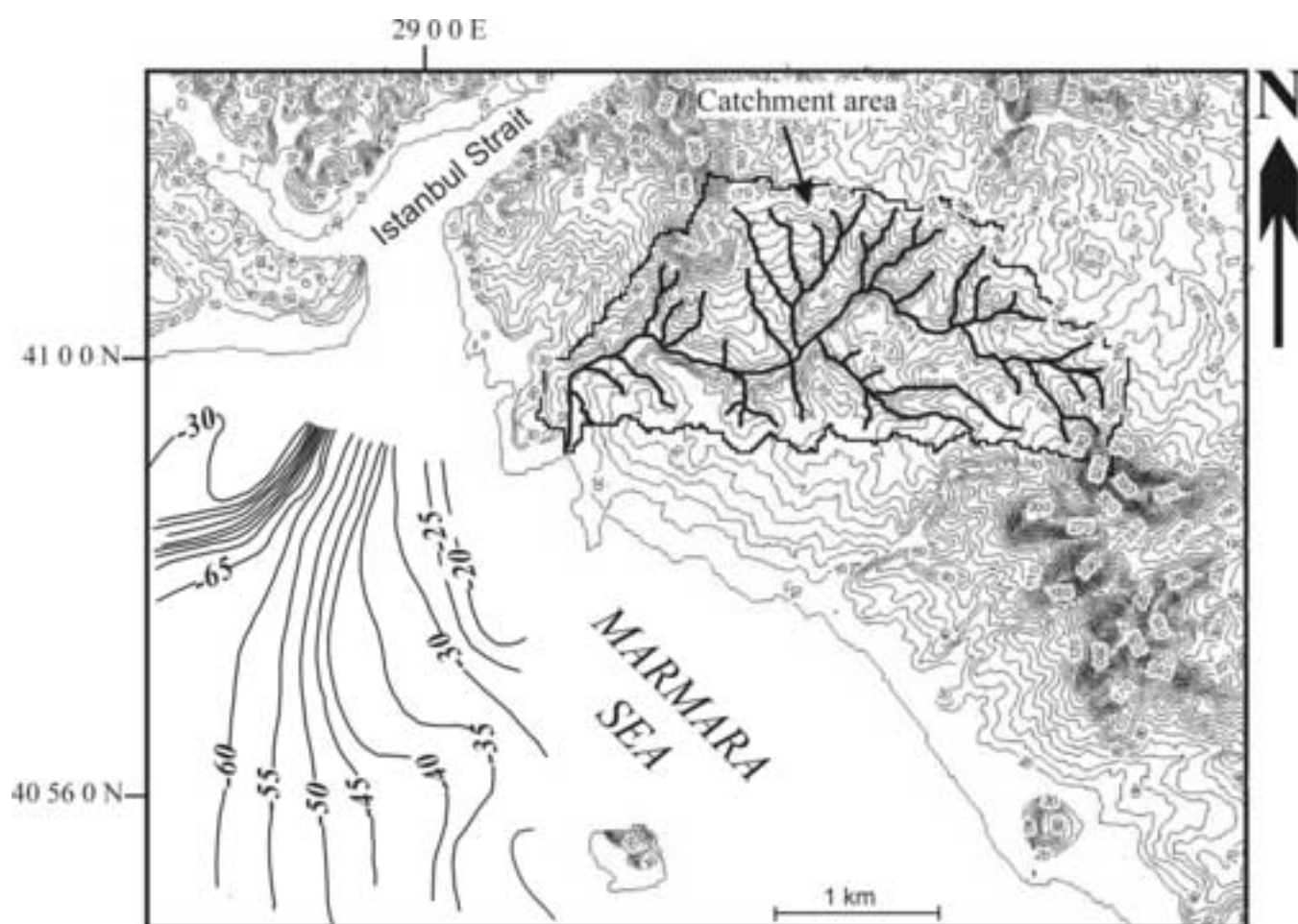


Figure 11

Figure 13

[Click here to download high resolution image](#)

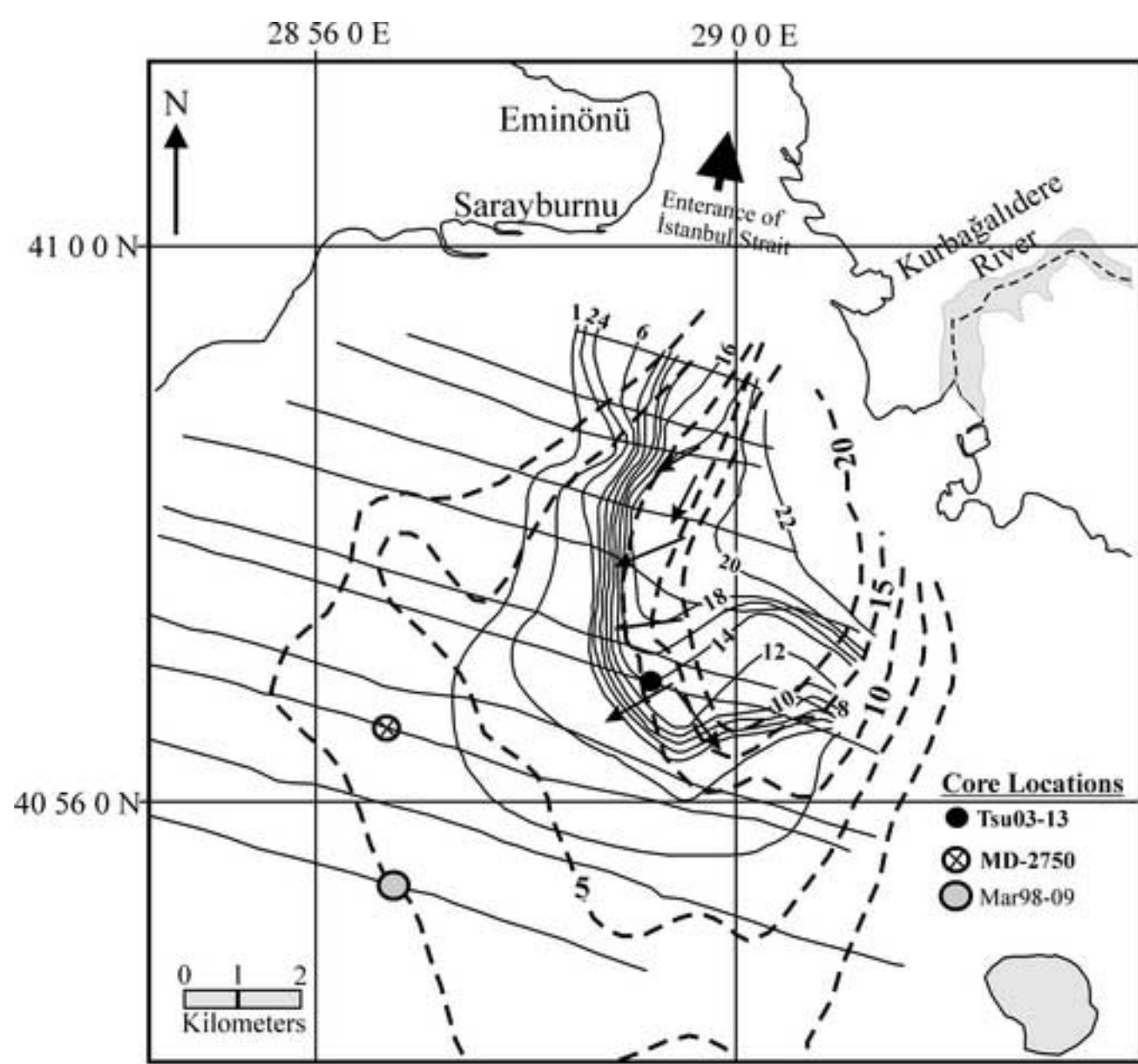


Figure 13

Figure 14
[Click here to download high resolution image](#)

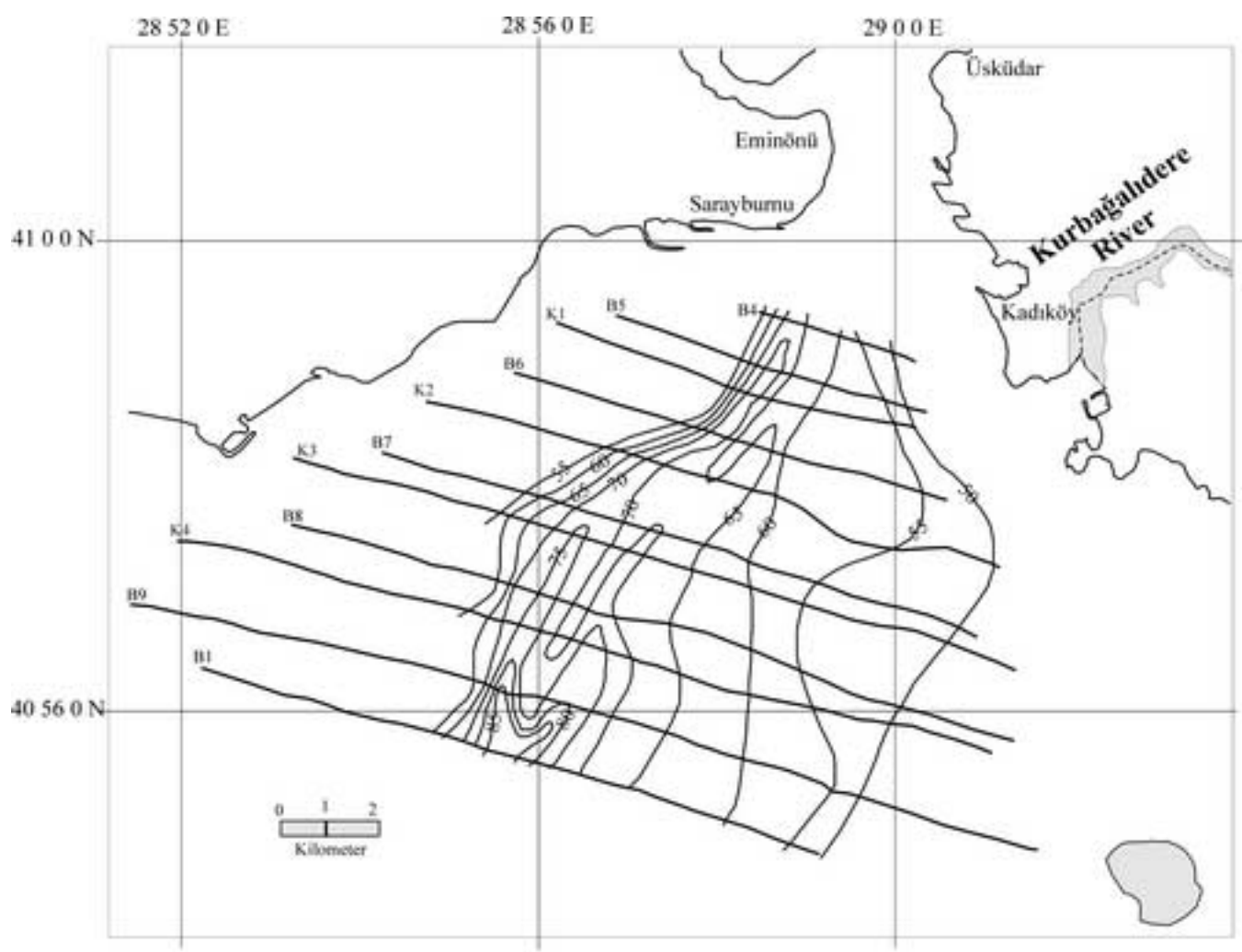


Figure 14

Figure 15

[Click here to download high resolution image](#)

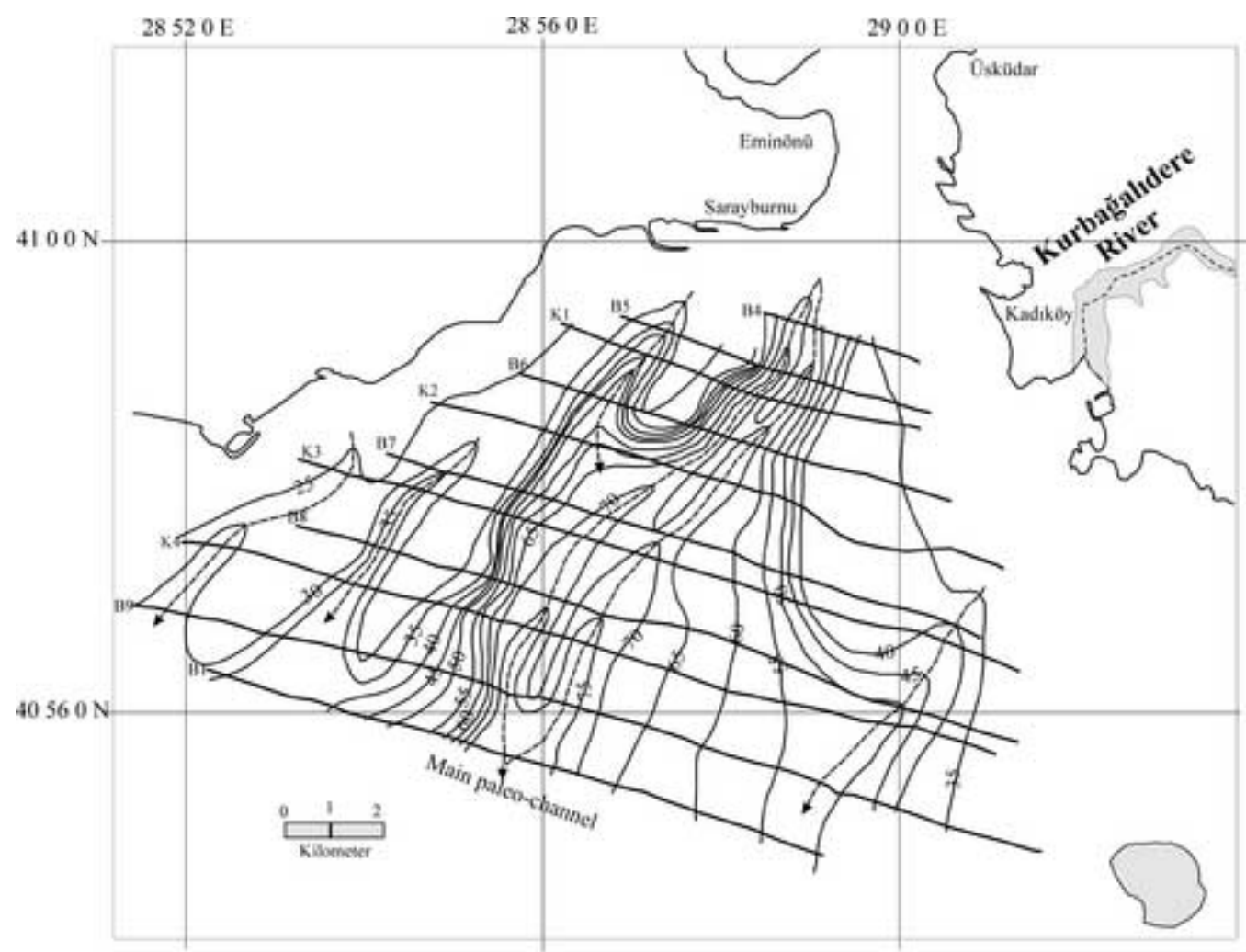


Figure 15

Table 1

Conventional dates in gravity cores recovered for this study (mbs, meter below surface;
mbsf, meter below sea floor)

Site, location, water depth (mbs), dated material (lab.number)	Unit	Core depth	Age (¹⁴C yr BP.)
Southern entrance to the Istanbul strait, Tsu03-13, -34m, mollusc (A-13668)	Unit 2	1.55 mbsf	4380(+100/-95)
Southern entrance to the Istanbul Strait, MD-2750, -68m, bivalve (OS- 50131)	Unit 3	3.56 mbsf	6460 +/- 55
Southern entrance to the Istanbul Strait, MD-2750, -68m, bivalve (OS- 53538)	Unit 5	11.26 mbsf	10450 +/- 50
Southern entrance to the Istanbul Strait, MD-2750, -68m, bivalve (OS- 50130)	Unit 6	12.36 mbsf	10900 +/- 65

Table 2[Click here to download Table: Table 2.doc](#)

Table 2. Mean discharge and suspended sediment discharge rates of rivers around Marmara and western Black Sea regions.

Rivers	Mean Discharge (m³/yr)	Suspended Sediment Discharge (t/yr)
Gönen River	477 x 10 ⁶	188 000
Devrenkani River	227 x 10 ⁶	177 760
Kocaçay River	633 x 10 ⁶	375 000
Soğanlı River	864 x 10 ⁶	1 210 000
Karasu River	142 x 10 ⁶	82 000
Boluçayı River	251 x 10 ⁶	140 000
Kurbağalıdere River	80 x 10 ⁶	60 000